Food Hydrocolloids 47 (2015) 146–157

Contents lists available at ScienceDirect

Food Hydrocolloids

journal homepage: www.elsevier.com/locate/foodhyd

Amaranth protein films reinforced with maize starch nanocrystals

Maria Cecilia Condés [a], María Cristina Añón [a], Adriana Noemi Mauri [a, *], Alain Dufresne [b, c]

[a] Centro de Investigación y Desarrollo en Criotecnología de Alimentos (CIDCA) – CCT La Plata, Facultad de Ciencias Exactas, Universidad Nacional de La Plata y Consejo Nacional de Investigaciones Científicas y Técnicas, Calle 47 y 116, 1900 La Plata, Argentina
[b] Univ. Grenoble Alpes, LGP2, F-38000 Grenoble, France
[c] CNRS, LGP2, F-38000 Grenoble, France

ARTICLE INFO

Article history:
Received 9 October 2014
Received in revised form
16 January 2015
Accepted 22 January 2015
Available online 3 February 2015

Keywords:
Bionanocomposites
Biodegradable films
Starch nanocrystals
Botanical origen
Amaranth proteins

ABSTRACT

The effect of the addition of starch nanocrystals – prepared from waxy and normal maize starch granules – to amaranth protein formulations on the physicochemical and structural properties of the resulting nanocomposite films was studied. All nanocomposites films were homogeneous, translucent and had similar thickness and optical properties than the neat protein film due to the good dispersion of the nanoreinforcements in the protein matrix and the good chemical affinity between both components. Nevertheless, the presence of nanocrystals affected differently the way in which protein matrix stabilized, according to the origin of the reinforcement: mainly by disulfide bonds for waxy maize nanocrystals and by hydrogen bonds for normal maize nanocrystals. This induced a different reinforcing effect for amaranth protein films, being more significant for normal maize nanocrystals that however presented a lower crystallinity. Moreover, nanocomposite films presented improved water vapor permeability (WVP), water uptake (WU), surface hydrophobicity and mechanical behavior than proteins films and also a delay in their weight loss in soil.

1. Introduction

Interest in biodegradable materials has increased during the past decades because of their potential applications and the possibility to contribute to solving environmental pollution. The use of biopolymers such as polysaccharides and proteins and of lipids, or their composites to prepare edible films and coatings holds promise for innovative applications in food protection and preservation. Numerous proteins such as corn zein, wheat gluten, soy, peanut, cottonseed, sunflower, rice bran, serum albumin, egg white, collagen, gelatin, myofibrils, casein and whey proteins, and others of limited availability, have been studied as potential film forming agents (Cuq, Gontard, & Guilbert, 1998; Gennadios, 2002; Krochta, 1997). These films are characterized by excellent barrier properties to oxygen, lipids and flavorings but they display poor mechanical properties, and high permeability to water vapor (Gennadios, 2002). It has been demonstrated that this functionality is determined by the film microstructure that varies significantly depending on the type and initial state of the protein, and the processing methodology (Denavi et al., 2009).

Amaranth is an ancestral crop with well-known agronomic advantages (Lehmann, 1996). Its small seeds contain proteins with a well-balanced composition in essential amino-acids and important content of sulfur-containing amino-acids (Bressani, 1989). Condés, Añón, and Mauri (2013) have studied the film formation from both native and thermally treated amaranth protein isolates. They observed that films prepared from treated proteins show better mechanical properties and lower solubility. It was attributed to interactions between polypeptide chains during film formation due to the unfolded conformation of treated amaranth proteins leading to a higher degree of cross-linking. This behavior was reflected in the higher tensile strength of this material and in the lower amount of water-soluble free peptides that remained linked to the matrix.

Another strategy to improve the functionality of protein films, especially their mechanical and barrier properties is the addition of nanoreinforcement to the formulation. Inorganic nanoparticles of various shapes, such as layered silicates, spherical SiO_2, or carbon nanotubes have been incorporated into soy protein formulations, for example, to enhance their performance (Ai, Zheng, Wei, & Huang, 2007; Chen & Zhang, 2006; Dean & Yu, 2005; Echeverría, Eisenberg, & Mauri, 2014; Yu, Cui, Wei, & Huang, 2007; Yu, Dean, & Li, 2006; Zheng, Ai, Wei, Huang, & Chang, 2007). Because of the safety concern of inorganic nanoparticles, there are quite

* Corresponding author. Tel.: +54 221 4249287; fax: +54 221 4254853.
E-mail address: anmauri@quimica.unlp.edu.ar (A.N. Mauri).

http://dx.doi.org/10.1016/j.foodhyd.2015.01.026
0268-005X/

interests in using biodegradable, biocompatible, and natural nanostructured objects, such as rod-like cellulose or chitin whiskers, and platelet-like starch nanocrystals (Angellier, Choisnard, Molina-Boisseau, Ozil, & Dufresne, 2004; Nair & Dufresne, 2003; Paillet & Dufresne, 2001; Putaux, Molina-Boisseau, Momaur, & Dufresne, 2003; Samir Azizi, Alloin, & Dufresne, 2005). In particular, starch nanocrystals have become a suitable alternative as nanoreinforcement due to their low cost and simple production method. Starch nanocrystals (SNC) are crystalline platelets resulting from the disruption of the semicrystalline structure of starch granules by the acid hydrolysis of amorphous parts. The addition of starch nanocrystals from different botanical origin to biodegradable films – waxy starch, soy protein, or polyvinyl alcohol – has improved barrier and mechanical properties of the resulting materials (Chen, Cao, Chang, & Huneault, 2008; García, Ribba, Dufresne, Aranguren, & Goyanes, 2009; Zheng, Ai, Chang, Huang, & Dufresne, 2009).

It is well known that the amylose:amylopectin content of starch greatly affects its structural and functional properties. The branch chain length of amylopectin has been related to starch crystallization (Hanashiro, Abe, & Hizukuri, 1996) and affects the gelatinization and pasting properties (Jane et al., 1999), but also the size, shape, crystallinity and rheological properties of their nanocrystals (LeCorre, Bras, & Dufresne, 2011).

The aim of this work was to study the effect of the addition of starch nanocrystals – prepared from native waxy and normal maize starch granules – to amaranth protein formulations, on the physicochemical properties of ensuing nanocomposite films, analyzing how the differences in both starches affect the nature of their corresponding nanocrystals and also their efficiency as reinforcement of amaranth protein films.

2. Experimental

2.1. Plant materials

Seeds of *Amaranthus hypochondriacus* (cultivar 9122) used in this work were obtained from Estación Experimental del Instituto Nacional de Tecnología Agropecuaria (INTA), Anguil, La Pampa, Argentina.

Both waxy and normal maize starches (Sigma-Aldrich, Germany) were used for nanocrystal preparation.

2.2. Amaranth flour preparation

Seeds were ground and screened by 0.092 mm mesh. The resulting flour was defatted with hexane at 25 °C for 5 h (100 g/L suspension) under continuous stirring. After drying at room temperature, the flour was stored in hermetic containers in a chamber at 4 °C up to a month, when it was used for protein isolate preparation.

2.3. Preparation of amaranth protein isolate

Amaranth protein isolate (**API**) used in this study was prepared according to Martínez and Añón (1996). Briefly, defatted flour was suspended in water (100 g/L) and the pH was adjusted to 11.0 with 2 N NaOH. The suspension was stirred for 60 min at room temperature and then centrifuged for 20 min at 9000 × *g* and 15 °C. The supernatant was adjusted to pH 5.0 with 2 N HCl and then centrifuged at 9000 × *g* for 20 min at 4 °C. The pellet was suspended in water, neutralized with 0.1 N NaOH and freeze-dried. API was stored in hermetic containers in a chamber at 4 °C up to two months until used.

2.4. Preparation of starch nanocrystals

Waxy maize and normal maize starch nanocrystals were obtained according to a previously described method (Angellier et al., 2004). Briefly, acid hydrolysis of 36.725 g of waxy or normal maize starch granules was performed in a 250 mL 3.16 M H_2SO_4 solution, at 40 °C and 100 rpm. The mixture was subjected to an orbital shaking action during 5 days. Subsequently, the ensuing insoluble residue was washed with distilled water and separated by successive centrifugations at 10,000 rpm and 5 °C, until neutrality. The aqueous suspensions of starch nanoparticles were stored at 4 °C after adding several drops of chloroform to inhibit the growth of microorganisms, or freeze-dried according to the requirements of each assay.

The hydrolysis yield (wt%) was calculated as the ratio between the weight of freeze-dried nanoparticles and the initial weight of native granules for an aliquot of 50 mL taken in the 250 mL of hydrolyzed suspensions. It was verified that these aliquots were representative of the entire volume of 250 mL.

2.5. Starch granule and nanocrystal characterization

2.5.1. Amylose content

Amylose content of the starch granules was determined by using the method of Williams, Kuzina, and Hlynka (1970). A starch sample (20 mg) was taken and 10 mL of 0.5 N KOH was added. The suspension was thoroughly mixed. The dispersed sample was transferred to a 100 mL volumetric flask and diluted to the mark with distilled water. An aliquot of tested starch solution (10 mL) was pipetted into a 50 mL volumetric flask and 5 mL of 0.1 N HCl was added followed by 0.5 mL of iodine reagent. The volume was diluted to 50 mL and the absorbance was measured at 625 nm. The measurement of the amylose content was determined from a standard curve developed using amylose and amylopectin blends.

2.5.2. Scanning electron microscopy (SEM) and field emission gun scanning electron microscopy (FEG-SEM)

A SEM 505 (Philips, Netherlands), with an accelerating potential of 10 kV was used to examine the morphology of starch granules. Starch samples were prepared by depositing granules on an aluminum stub using double-sided adhesive tape and the sample was coated with gold (Sputter coater, Edwards S150B).

SEM observation performed using a Zeiss DSM982 Gemini with a field emission gun (FEG) was used to examine the morphology of starch nanoparticles. All samples were prepared by depositing 2.5 μL of starch nanocrystal suspension (with concentration 0.0001% w/v) on a TEM grid.

2.5.3. X-ray diffraction

Normal and waxy maize starch nanocrystals were submitted to X-ray radiation using a diffractometer (Philips model PW 1510), with a vertical goniometer operating at Cu Kα radiation wavelength (λ = 0.154 nm), 40 kV, 30 mA and sampling interval of 0.01°. Scattered radiation was detected in the angular range 2θ = 5–40°.

The crystallinity index of the samples was quantitatively estimated following the method of Nara and Komiya (1983) adapted, also called the “two-phase” method. A curve connecting the peaks baseline was plotted on the diffractogram. The area above the curve was assumed to correspond to the crystalline domains, and the lower area to the amorphous part. The ratio of upper area to total area was taken as the crystallinity index.

2.5.4. Differential scanning calorimetry (DSC)

A TA Instrument DSC Q100 V9.8 Build 296 (New Castle, DE, USA) was used to determine the thermal characteristics of starch

granules and nanocrystals. Temperature and heat flow calibration of the equipment was carried out according to ASTM standards, using lauric and stearic acids, and indium as standards, respectively. For starch granules, hermetically sealed aluminum pans containing 15 mg of starch dispersion (30% w/v in distilled water) were prepared and scanned at 10 °C/min over the range 20–135 °C. For starch nanocrystals, hermetically sealed aluminum pans containing 5 mg of freeze-dried starch nanocrystals were prepared and scanned at 10 °C/min over the range 0–300 °C. Gelatinization and fusion enthalpies (ΔH_{gel} and ΔH_f), and peak temperatures (T_{gel} and T_f) were determined from the corresponding thermograms (Universal Analysis V4.2E, TA Instruments, New Castle, DE, USA). Enthalpy values were expressed as J/g of starch or nanocrystal, taking into account the dry weight, determined by perforating the pans and heating overnight at 105 °C.

2.5.5. Particle size determination

The determination of starch nanocrystal size by measuring dynamic light scattering (DLS) was made on a Zetasizer Nano-Zs (Malvern Instruments Ltd., United Kingdom) equipped with a He–Ne laser (633 nm) and a digital correlator (ZEN3600) with a measuring range of 0.6–6000 nm. Measurements at a scattering angle of 173° were performed at room temperature using a polystyrene cell. Nanocrystal dispersions were diluted to 0.05% v/v in milliQ water, thus eliminating the possible turbidity that may exist in the sample at higher concentrations. The sample was illuminated with a laser and the intensity of scattered light produced by the particles fluctuated at a rate that depends on particle size. Therefore, using the software provided with the equipment it was possible to obtain the particle size distribution by intensity, determining the average size and the polydispersity index that is the width of the Gaussian bell and reflects the diversity of particle size in the sample. All determinations were performed at least in triplicate.

2.6. Film formation

Films were prepared by casting dispersions of amaranth protein isolate (API, 5% w/v), glycerol (1.25% w/v, Anedra, Argentina) and variable amounts of normal or waxy maize nanostarch dispersions (0, 3, 6, 9 and 12 wt% relative to protein isolate mass) in distilled water. All dispersions were magnetically stirred for 1 h at room temperature, their pH was adjusted to 10.5 with 2 mol/L NaOH, and they were stirred again for additional 20 min. 10 mL of each film forming dispersion were poured onto polystyrene Petri dishes (64 cm^2) and dried at 40 °C for 4 h in an oven with air flow and circulation (Yamato, DKN600, USA). The dry films were conditioned at 20 °C and 58% relative humidity in desiccators with saturated solutions of NaBr for 48 h before being peeled from the casting surface for characterization.

2.7. Film characterization

2.7.1. Moisture content (MC)

MC was gravimetrically determined after drying in an oven at 105 °C for 24 h. Small film specimens collected after conditioning, were cut and placed on Petri dishes that were weighed before and after oven drying. MC values were determined in triplicate for each film, and calculated as the percentage of weight loss based on the original weight (ASTM D644-94, 1994).

2.7.2. Film thickness

Film thickness was measured by a digital coating thickness gauge (Check Line DCN-900, USA). Measurements were done at five positions along the rectangular strips for tensile test, and at the center and at eight positions round the perimeter for the WVP determination. The mechanical properties and WVP were calculated using the average thickness for each film replicate.

2.7.3. Film color

Film color was determined using a Minolta Chroma meter (CR 300, Minolta Chroma Co., Osaka, Japan). A CIE Lab color scale was used to measure the degree of lightness (L), redness (+a) or greenness (−a), and yellowness (+b) or blueness (−b) of the films. The instrument was standardized using a set of three Minolta calibration plates. Films were measured on the surface of the white standard plate with color coordinates of L = 97.3, a = 0.14 and b = 1.71. Total color difference (ΔE) was calculated from:

$$\Delta E = \sqrt{\left(L_{film} - L_{standard}\right)^2 + \left(a_{film} - a_{standard}\right)^2 + \left(b_{film} - b_{standard}\right)^2} \quad (1)$$

Values were expressed as the means of nine measurements on different areas of each film.

2.7.4. Opacity

Each film specimen was cut into a rectangular piece and placed directly in a spectrophotometer test cell, and measurements were performed using air as the reference. A spectrum for each film was obtained in an UV–Vis spectrophotometer (Beckman DU650, Germany). The opacity of the film (1/mm) was calculated by dividing the absorbance at 500 nm by the film thickness (mm) (Cao, Fu, & He, 2007). All determinations were performed in triplicate.

2.7.5. Mechanical properties

The tensile mechanical behavior was analyzed with a RSA3 (TA Instruments, USA) with a load cell of 100 N. Experiments were performed at room temperature, 25 °C, with a cross head speed of 50 mm/min. The sample dimensions were 10 × 5 × 1 mm^3, and the results were averaged on five measurements. The tensile strength and elongation at break were determined directly from the stress–strain curves, and the Young's modulus was calculated as the steepest slope of the initial linear portion of this curve to exclude the very initial strain that could be due to machine and clamp realignment artifacts.

2.7.6. Solubility in water

Solubility was measured by immersion of film disks (2.0 cm in diameter) in water containing sodium azide, at 25 ± 2 °C for a period of 24 h (Gontard, Guilbert, & Cuq, 1992). The amount of dry matter in the initial and final samples was determined by drying the samples at 105 °C for 24 h. All determinations were performed in triplicate.

2.7.7. Water vapor permeability (WVP)

Water vapor permeability tests were conducted using ASTM method E96-00 (ASTM E96-00, 1996) with some modifications (Gennadios, McHugh, Weller, & Krochta, 1994). Each film sample was sealed over a circular opening of 0.00177 m^2 in a permeation cell that was stored at 25 °C in a desiccator. To maintain a 75% relative humidity (RH) gradient across the film, anhydrous silica (0% RH) was placed inside the cell and a saturated NaCl solution (75% RH) was used in the desiccator. The RH inside the cell was always lower than outside, and water vapor transport was determined from the weight gain of the permeation cell. When steady-state conditions were reached (about 1 h), eight weight measurements were made over 5 h. Changes in the weight of the cell were recorded and plotted as a function of time. The slope of each line was calculated by linear regression and the water vapor

transmission rate (WVTR) was calculated from the slope (g/s H_2O) divided by the cell area (m^2). WVP (g/Pa s m) was calculated as:

$$WVP = [(WVTR) \times d] \Big/ \left[P_v^{H_2O} \times (RH_d - RH_c) \times A\right] \quad (2)$$

where $P_v^{H_2O}$ = vapor pressure of water at saturation (Pa) at the test temperature (20 °C), RH_d = RH in the desiccator, RH_c = RH in the permeation cell, A = permeation area (m^2), and d = film thickness (m). Each WVP value represents the mean value of at least three sampling units taken from different films.

2.7.8. Measurement of surface hydrophobicity

Surface hydrophobicity was assessed by measuring contact angle using a goniometer ramé-hart Model 500 (ramé-hart instrument co., USA). A 5 μL drop of demineralized water was placed on the surface of the film with an automatic piston syringe and photographed. An image analyzer was used to measure the angle formed between the base, constituted of the surface of the film in contact with the water drop, and the tangent to the water drop. The mean hydrophobicity value for the surface of each film was calculated from six measurements on the film.

2.7.9. Water uptake (WU)

The water uptake was determined used 1 cm^2 samples of rectangular films. After weighing to determine the initial weight (m_0), they were placed in a container conditioned at 98% RH using a saturated copper sulfate solution. At specific time intervals, the sample weight (m_t) was determined until an equilibrium value (m_∞) was reached. Three replicates were tested for each sample. The water uptake (WU%) of the sample was calculated as:

$$WU\% = (m_\infty - m_0) \times 100/m_0 \quad (3)$$

2.7.10. Differential solubility of proteins

Protein solubility of the films was determined according to the method described by Mauri and Añón (2006), with some modifications. Pieces of films were weighted and placed into a tube containing 1 mL water or buffer. Five different buffer systems all at pH 7.5 were used: a) 0.1 mol/L phosphate buffer (NaH_2PO_4) containing 0.1 mol/L NaCl (PB); b) PBD buffer: PB with 0.1% sodium dodecyl sulfate (SDS, Anedra, Argentine); c) PBU buffer: PB with 6 mol/L urea (Riedel-deHaën, Germany); d) PBDU buffer: PB with 0.1% SDS and 6 M urea, and e) PBDUM buffer: PB with 0.1% SDS, 6 mol/L urea and 2.5% 2-mercaptoethanol (ME, Sigma-Aldrich, Germany). The tubes were shaken for 24 h at 20 °C. Suspensions were then centrifuged at 9000 × *g* for 20 min at room temperature and the protein content in the supernatant was determined using a Bradford assay (Bradford, 1976). Standard curves using bovine serum albumin (BSA, Sigma-Aldrich Chemical Co., St. Louis, USA) were constructed for each buffer. For each type of film, at least two samples from four independent film preparations were solubilized. The soluble protein content was expressed as a percentage of the total amount of protein in the film, which was measured by the Kjeldahl method (AOAC 920.53, 1995).

2.7.11. Glass transition temperature (T_g)

The glass transition temperature (T_g) was determined by differential scanning calorimetry, using a DSC TA 2010 calorimeter Q100 V9.8 Build 296 (TA Instrument, New Castle, Del., USA) controlled by a TA 5000 module with a quench-cooling accessory. Temperature and heat flow calibration of the equipment were carried out according to ASTM Standards, using lauric and stearic acids, and indium as standards. Hermetically sealed aluminum pans containing 5–10 mg of films were prepared, and the capsules were scanned at 20 °C/min over the range −100 to 130 °C modulated. The glass transition temperature (T_g) was considered to be the inflexion point of the base line, caused by the discontinuity of the specific heat of the sample, and it was calculated with the help of the Universal Analysis V4.2E software (TA Instruments, New Castle, Del., USA) (Sobral, Menegalli, Hubinger, & Roques, 2001). All the assays were performed at least in duplicate.

2.7.12. Weight loss measurement

Weight loss measurement of films in soil was carried out as previously reported (Dalev, Patil, Mark, Vassileva, & Fakirov, 2000). Soil was taken from the surface layer. All inert materials were removed to obtain a homogeneous mass. 100 g soil was poured into a plastic pot up to a thickness of about 4 cm. Nanocomposite samples were accurately weighed. The samples were previously dried at 50 °C for 24 h. They were buried in the pots to a depth of 2 cm. Water was sprayed once a day to sustain the moisture. The samples were weighed every week for 3 weeks. After each period the samples were carefully taken out, washed with distilled water, and dried at 50 °C for 24 h and then weighed.

2.8. Statistical analysis

Results were expressed as mean ± standard deviation and were analyzed by analysis of variance (ANOVA). Means were tested with the Fisher's least significant difference test for paired comparison, with a significance level $\alpha = 0.05$.

3. Results and discussion

3.1. Maize starch granules and nanocrystals characterization

This study was carried with two maize starches with different amylose:amylopectin ratios, i.e. normal and waxy type. Some structural and physicochemical characteristics of the starch granules used are shown in Table 1. Both starches showed angular shape, presenting some “pin holes” and equatorial grooves or furrows (Fig. 1A), with sizes around 15–20 μm as shown by Sandhu, Singh, and Kaur (2004). These granules are mainly differentiated in the amylose content (Table 1) that was higher for normal maize starch (38.1%) than for waxy maize starch (1.6%), as expected according to Morrison, Milligan, and Azudin (1984).

Differences in amylose:amylopectin ratio in the granule influenced the crystallinity, calculated from the X-ray patterns as shown in Fig. 2. Waxy maize starch showed significantly higher crystallinity than normal maize starch (38.6 ± 0.9% and 20.8 ± 1.5%, respectively). Tang, Mitsunaga, and Kawamura (2006) reported that the backbone of the granule crystal structure is formed by amylopectin, with the amylose molecules randomly arranged individually, dispersed among amylopectin, in both crystalline and

Table 1
Structural and physicochemical characteristics of normal and waxy maize starch granules.

	Normal maize	Waxy maize
Granular diameter (μm)	15.9 ± 0.6[a]	16.1 ± 5.5[a]
Amylose content %	38.1 ± 1.9[a]	1.6 ± 0.3[b]
Crystalline type	A/V	A
Crystallinity %	20.8 ± 1.5[a]	38.6 ± 0.9[b]
T_{gel} (°C)	71.0 ± 0.1[a]	70.9 ± 0.2[a]
ΔH_{gel} (J/g)	13.8 ± 1.6[a]	17.3 ± 0.5[b]

All values were average ± SD from two or more values. Reported average values for all parameters within a line with same superscripts (*a* and *b*) are not significantly different ($P < 0.05$).

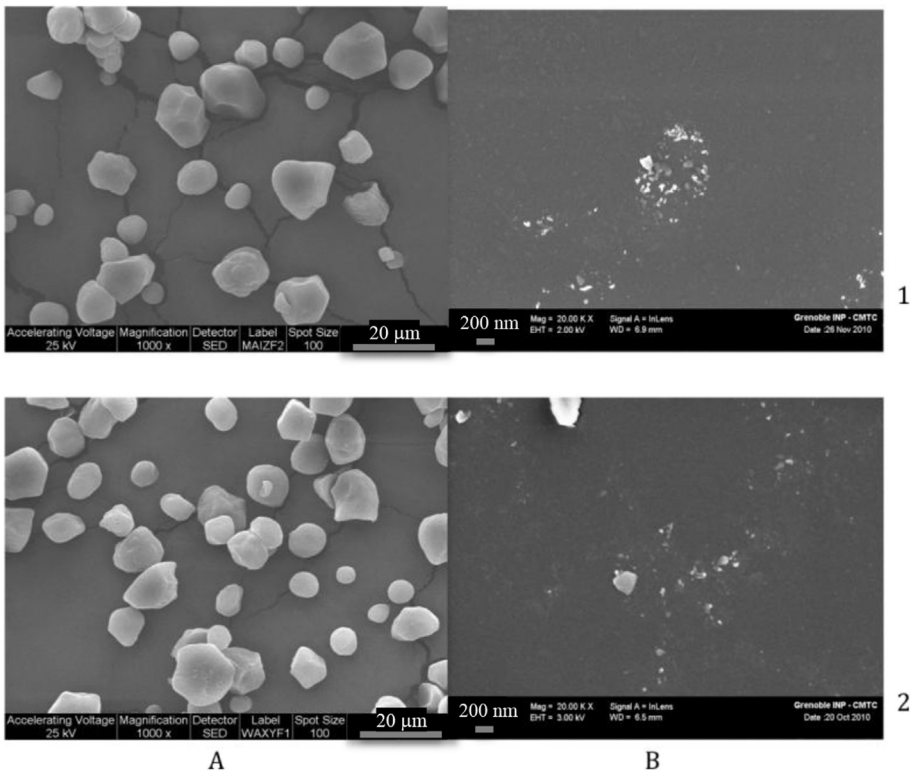

Fig. 1. SEM of starch granules (A) and FEG-SEM of starch nanocrystals (B) for normal maize starch (1) and waxy maize starch (2).

amorphous regions (Oates, 1997). The X-ray diffraction patterns for both maize starch granules showed single broad peaks at $2\theta = 23.2°$ and 15°, and dual peaks at $2\theta = 17–18.1°$ which correspond to A-type pattern typical from cereal starches (Singh, Inouchi, & Nishinari, 2006). For the normal maize starch pattern an additional peak at 20° was also observed, which could be attributed to the amylose–lipid complex, composed of fatty acids and amylose (French, 1984) that are generally in the amorphous phase of the granule. This complex is typical of wheat starch and some genotypes of maize starch, as shown by Zobel (1988) and Singh et al. (2006) and this complex is known as V-type.

The gelatinization temperature obtained from DSC thermograms, and shown in Table 1, was similar for both starches, although the gelatinization enthalpy of waxy maize starch was higher than the one corresponding to normal maize starch. This might be attributed to the fact that starches with long amylopectin branch chain length, and consequently higher crystallinity, displayed higher structural stability of the granule, resulting in a higher resistance to gelatinization (Barichello, Yada, Coffin, & Stanley, 1990; Singh, Singh, Kaur, Sodhi, & Gill, 2003). This is consistent with previous studies where it has been reported that the gelatinization and swelling properties of the granule are largely

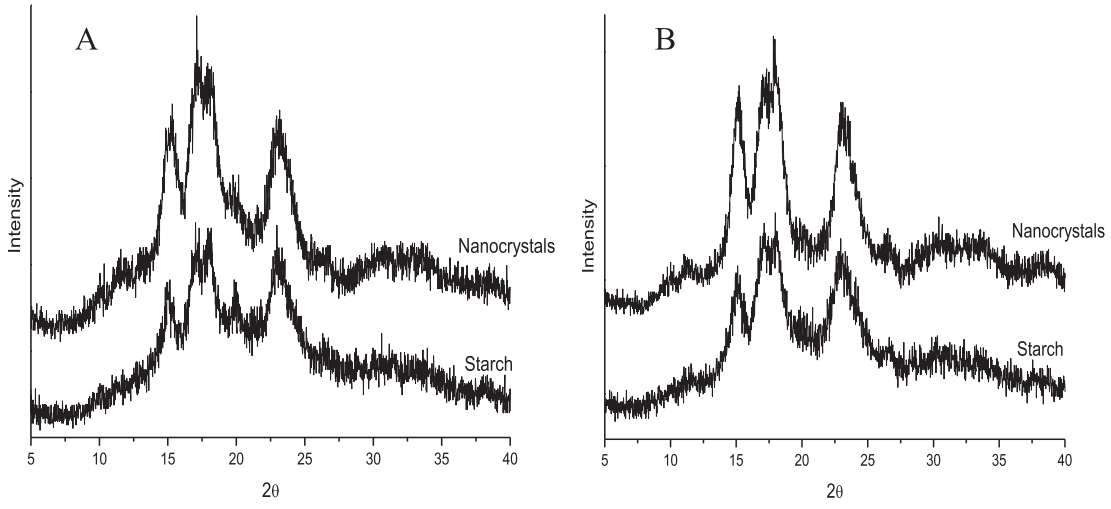

Fig. 2. XRD patterns for normal (A) and waxy maize (B) starch and corresponding starch nanocrystals.

controlled by the molecular structure of amylopectin (chain length, degree of branching, molecular weight and polydispersity), by the granule composition (amylose:amylopectin ratio and phosphorus content), and granule architecture (relation between amorphous and crystalline region) (Tester, 1997). In these thermograms, the endotherm attributable to the melting of amylose–lipid complex is not observed, although its presence was suggested from the X-ray pattern and it was reported by other authors for wheat starch (Yoo & Jane, 2002). This absence of endotherm in the thermogram could be attributed to the higher stability of the complex V to temperatures near 130 °C, as shown by Zobel, Young, and Rocca (1988), or to the fact that the amount of complex is very low, not allowing detection with this method.

Nanocrystals were obtained from these starch granules, by acid hydrolysis process under conditions previously optimized, in order to obtain more stable nanocrystals with smaller sizes, better yields and shorter hydrolysis time (Angellier et al., 2004; LeCorre, Bras, & Dufresne, 2010). Hydrolysis yield of nanocrystals was 24.4 wt% and 17.0 wt% for normal and waxy maize starch, respectively, according with Angellier et al. (2004). Fig. 1B shows FEG-SEM micrographs obtained for the starch nanocrystals. All nanocrystals exhibit a size below 200 nm, showing a size modification after acid hydrolysis of the starch granules. The detailed investigation on the structure of these hydrolyzed residues by TEM showed that they consisted of platelet-like nanoparticles (Putaux et al., 2003). Such nanocrystals are generally observed in the form of aggregates (Angellier, Molina-Boisseau, & Dufresne, 2005; Angellier, Putaux, Molina-Boisseau, Dupeyre, & Dufresne, 2005). The average size and polydispersity index of these aggregates determined by DLS are reported in Table 2. The obtained average sizes show the tendency of nanocrystals to form aggregates, since from microscopic observations (Fig. 1B) smaller sizes than those obtained by this method were reported. This trend can be attributed to the large surface area of the platelets and to the association through the formation of hydrogen bonds between hydroxyl groups, which are found in a substantial number for single area of nanocrystals, according to Garcia et al. (2009). Similar trend of aggregation has also been reported for other nano-reinforcements obtained from polysaccharides, such as cellulose nanofibers (Eichhorn et al., 2010; Ljungberg et al., 2005). The nanocrystal aggregates formed from both maize starches had a monomodal distribution, indicating the presence of a single population of particles in both dispersions, at least in the detection range employed. Normal maize nanocrystals showed a smaller intermediate size but a higher polydispersity than those from waxy.

Fig. 2 shows the X-ray diffraction patterns for nanocrystals from normal and waxy maize together with their corresponding native granules for comparison. As previously reported in the literature, although being called nanocrystal, these nanoparticles are rather partially crystalline, since amorphous regions remain after hydrolysis, as observed in the diffractograms. Both starch nanocrystals retained A-type pattern of starch granules, with peaks at 23°, 17–18.1° and 15°, with no evidence of additional or missing crystalline structure with respect to the granules. The crystallinity for normal maize starch increased slightly after hydrolysis, while for waxy maize starch, the crystallinity of the nanocrystals showed no significant difference with the granules. Theoretically, the degree of crystallinity (ratio between the mass of crystalline domains and the total mass of nanocrystal) of starch nanocrystals should be 100%, but actually incomplete removal of amorphous regions and less ordered surface chains may result in a lower degree of crystallinity. The values commonly reported in the literature are within the range 45–50 % (Lin, Huang, & Dufresne, 2012). However, higher values such as 79% after 10 days hydrolysis have been reported (Duan, Sun, Wang, & Yang, 2011). Increased crystallinity for normal maize starch could be attributed to the fact that hydrolysis of the amorphous regions was more efficient, leading to the increase of the relative crystallinity, a fact which was not significant for waxy maize starch possibly due to the lower amount of amorphous regions in the granules. It should be noted that when the degree of crystallinity of the nanocrystals is not increased compared to the starch granules, the procedure could be better consider as a starch "fragmentation" method, in which the final particles are just small fragments of similar composition. Nevertheless, we still used the common term nanocrystal to describe acid-hydrolyzed starch residues.

Contrarily, LeCorre, Bras, and Dufresne (2012) showed an increase in crystallinity after hydrolysis for waxy maize starch, as well as for corn, wheat and potato starch, without finding any relationship to the content of amylopectin, crystalline type and botanical origin of granules. These authors expected a greater increase in crystallinity for starches with higher amylopectin contents, given that they had less amorphous regions susceptible to hydrolysis. However, they attributed this behavior to two possible causes: (i) the optimization of the hydrolysis process was carried out for waxy maize starch, and may not be the appropriate process for other starches; and (ii) hydrolysis of crystallites defective in amylopectin by the extension of the process, which would induce solubilization of the crystal structure. Some of these causes can be responsible for the invariance of the crystallinity of waxy maize upon hydrolysis. Also, LeCorre et al. (2011) showed that, despite the

Table 2
Structural and physicochemical characteristics of normal and waxy maize starch nanocrystals.

		Normal maize	Waxy maize
Aggregate average size (nm)		823 ± 9[a]	1287 ± 125[b]
Aggregate polydispersity index		0.25	0.11
Crystalline type		A/V	A
Crystallinity %		26.3 ± 0.9[a]	41.1 ± 2.3[b]
T_f (°C)	Endotherm 1	189.1 ± 4.0[a]	175.3 ± 6.2[a]
	Endotherm 2	252.2 ± 2.2[a]	238.9 ± 3.0[b]
ΔH_f (J/g)	Endotherm 1	152.0 ± 20.3[a]	169.0 ± 12.4[a]
	Endotherm 2	10.3 ± 2.8[a]	31.7 ± 3.3[b]

All values were average ± SD of two or more values. Reported average values for all parameters within a line with same superscripts (*a* and *b*) are not significantly different ($P < 0.05$).

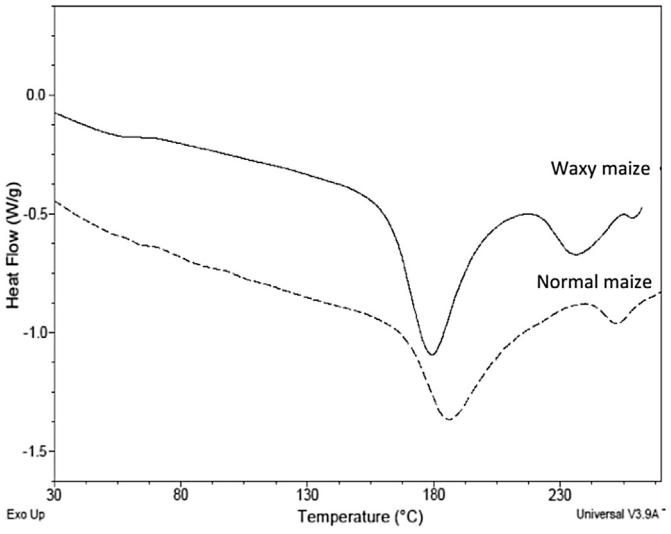

Fig. 3. DSC thermograms for normal and waxy maize starch nanocrystals.

Table 3
Thickness and water content of amaranth protein isolate films with the addition of different contents of normal and waxy maize starch nanocrystals.

	Starch nanocrystal content (wt%)	Thickness (μm)	Water content (%)
Control	0	69 ± 15[a]	19.1 ± 0.6[a]
Normal maize	3	63 ± 11[a]	18.8 ± 1.0[a]
	6	91 ± 14[a]	20.6 ± 0.5[a]
	9	58 ± 9[a]	20.6 ± 1.0[a]
	12	71 ± 12[a]	18.6 ± 0.8[a]
Waxy maize	3	70 ± 16[a]	18.6 ± 1.7[a]
	6	73 ± 15[a]	22.8 ± 0.6[b]
	9	75 ± 13[a]	20.1 ± 0.7[a]
	12	74 ± 8[a]	15.2 ± 0.2[c]

All values were average ± SD of two values. Reported average values for all parameters within a column with same superscripts (*a*, *b* and *c*) are not significantly different ($P < 0.05$).

observed increase in crystallinity, this parameter presents low values for all nanocrystals, showing that a significant amount of unorganized material remained in the nanocrystal suspension.

DSC thermograms of normal and waxy maize starch nanocrystals are shown in Fig. 3. Two endotherms were observed in these thermograms for both nanocrystals, which could be attributed to differences in the thermal stability of nanocrystals: a less resistant population that melts first and another comprising more stable crystals melting therefore at higher temperatures. The temperatures and enthalpies of fusion for each endotherm are reported in Table 2. While no significant differences in these properties were observed for the first endotherm, the width of this transition was significantly higher for nanocrystals obtained from normal maize starch especially due to an elongation of the peak at higher temperatures. But the second endotherm was different for both types of studied nanocrystals. Waxy maize nanocrystals showed a lower transition temperature and a higher enthalpy than normal maize nanocrystals for this last transition. Considering that starch nanoparticles are only semi-crystalline, the differences found in the temperature and enthalpy between both studied nanocrystals could be due to various causes, including the formation of a more or less perfect crystal, or different water content, as suggested by LeCorre et al. (2012). Thielemans, Belgacem, and Dufresne (2006) and LeCorre et al. (2012) also observed two endotherms at about 150 and 200 °C when analyzing lyophilized waxy maize nanocrystals by DSC, and suggested that it does not seem to be a correlation between the temperature of the thermal transition and the original amylose content of the granules or crystalline type.

Table 4
Hunter color values (L, a and b), total color difference (ΔE) and opacity of amaranth protein isolate films with the addition of different contents of normal and waxy maize starch nanocrystals.

Starch nanocrystal content (wt%)		Hunter-lab color parameters				Opacity (1/mm)
		L	a	b	ΔE	
Control	0	83.5 ± 1.4[a]	−0.1 ± 0.1[a]	10.2 ± 2.6[a]	16.2 ± 2.6[a]	2.6 ± 0.7[a]
Normal maize	3	84.5 ± 1.4[a]	0.0 ± 0.1[a]	10.0 ± 3.2[a]	15.4 ± 2.9[a]	2.9 ± 1.1[a]
	6	83.3 ± 1.2[a]	−0.2 ± 0.1[a]	12.0 ± 2.2[a]	17.4 ± 2.1[a]	2.2 ± 0.4[a]
	9	82.6 ± 1.4[a]	−0.2 ± 0.1[a]	11.9 ± 2.5[a]	17.9 ± 2.6[a]	2.2 ± 0.9[a]
	12	82.5 ± 1.2[a]	−0.1 ± 0.1[a]	13.8 ± 2.5[a]	20.2 ± 4.0[a]	2.2 ± 0.8[a]
Waxy maize	3	81.5 ± 1.7[a]	−0.1 ± 0.2[a]	13.2 ± 2.8[a]	19.6 ± 2.9[a]	2.1 ± 0.4[a]
	6	80.7 ± 1.7[a]	−0.2 ± 0.1[a]	14.5 ± 2.8[a]	21.0 ± 3.0[a]	2.2 ± 0.5[a]
	9	79.7 ± 1.3[a]	−0.1 ± 0.2[a]	16.1 ± 1.6[a]	22.7 ± 2.0[a]	2.6 ± 0.7[a]
	12	81.1 ± 0.6[a]	−0.2 ± 0.1[a]	14.1 ± 1.1[a]	20.5 ± 1.0[a]	2.1 ± 0.2[a]

All values were average ± SD of two values. Reported average values for all parameters within a column with same superscripts (*a*) are not significantly different ($P < 0.05$).

It is worth highlighting that although the crystallinity of normal maize starch granule is lower than that of waxy maize starch, the hydrolysis yield for the former is higher, and the crystallinity of the nanocrystals even greater than the granule itself.

3.2. Films characterization

3.2.1. Appearance

Nanocomposite films prepared by casting with different concentrations of normal and waxy maize starch nanocrystals were homogeneous, translucent and slightly brownish, with a general visual appearance similar to the control amaranth protein film. Furthermore, all the studied films had similar thickness and optical properties – color and opacity – as it is shown in Tables 3 and 4. The fact that the presence of nanocrystals did not affect the degree of compaction of the material, and its coloration and opacity, could be attributed to a good dispersion of the nanoreinforcement in the protein matrix due to the expected good chemical affinity between both components. Petersson and Oksman (2006) suggested that the degree of exfoliation and volume fraction of the nanoreinforcement has a large influence on the UV and visible light transmittance. They reported that the absence of reduction in the amount of light being transmitted through the nanocomposite film is an indication that the nanoreinforcement is fully exfoliated. As a result there should not be a large difference in the amount of light being transmitted through the nanocomposite films compared to the pure matrix.

3.2.2. Water susceptibility

The water content of films, shown in Table 3, was around 20% for all studied formulations. The presence of normal maize nanocrystals did not modify significantly the water content of the protein film, while the addition of waxy maize nanocrystals showed an increase in this property at intermediate concentrations (6 wt%) with a decrease at higher concentrations, although these changes were not very important.

Table 5 reports the water solubility, water vapor permeability (WVP), water uptake (WU), and contact angle values for films with different starch nanocrystal concentrations.

The WVP value obtained for amaranth protein film was one order of magnitude lower than the one corresponding to other proteins. This result might be attributed to the hydrophobic nature of amaranth protein, particularly that of 11S and P-globulins that are present in these isolates (Konishi & Yoshimoto, 1989). WVP of the films reinforced with normal maize starch nanocrystals

Table 5
Water vapor permeability (WVP), water uptake (WU), water solubility and contact angle for films prepared from amaranth protein isolate and normal and waxy maize starch nanocrystals.

	Starch nanocrystal content (wt%)	WVP*10^{-11} (g H_2O/Pa m s)	WU (%)	Solubility (%)	Contact angle (°)
Control	0	3.0 ± 0.2[a]	95.0 ± 2.9[a]	78.6 ± 2.3[a]	47.6 ± 10.9[a]
Normal maize	3	2.1 ± 0.3[b]	92.2 ± 3.3[a]	81.3 ± 3.2[a]	Not determined
	6	2.8 ± 0.6[a]	59.3 ± 3.1[b]	82.3 ± 3.2[a]	70.3 ± 3.8[b]
	9	2.1 ± 0.5[b]	63.0 ± 5.1[b]	78.5 ± 1.3[a]	Not determined
	12	1.9 ± 0.2[b]	55.3 ± 2.7[b]	92.1 ± 1.6[b]	31.4 ± 9.7[a]
Waxy maize	3	2.3 ± 0.2[b]	63.9 ± 4.5[b]	84.6 ± 3.3[a]	Not determined
	6	2.1 ± 0.4[b]	71.2 ± 14.6[b]	75.1 ± 2.1[a]	80.9 ± 10.3[b]
	9	2.4 ± 0.6[b]	78.1 ± 11.2[b]	71.3 ± 0.9[a]	Not determined
	12	3.3 ± 0.8[a]	62.3 ± 12.8[b]	71.4 ± 3.2[a]	81.1 ± 8.9[b]

All values were average ± SD of two values. Reported average values for all parameters within a column with same superscripts (*a* and *b*) are not significantly different ($P < 0.05$).

decreased for all formulations, except with the addition of 6 wt% nanocrystals. However, WVP decreased upon the addition of waxy maize starch nanocrystals until 9 wt%, while it increased for 12 wt%. LeCorre et al. (2010) and Kristo and Biliaderis (2007) proposed that at lower nanoparticle contents a better dispersion and lower aggregation of starch nanocrystals occurred, contributing to generate a tortuous path for the passage of water molecules provoking a decrease in WVP. For higher nanoparticle contents their tendency to aggregate increases and a reduction of the effectiveness of this effect besides the hydrophilic nature of the nanocrystals leads to increase WVP. These results agree with those reported by García et al. (2009) which showed that the WVP decreased approximately 40% with the addition of 2.5 wt% cassava starch nanocrystals to a cassava starch matrix.

WU of amaranth protein films significantly decreased with the addition of starch nanocrystals. Considering that both components, starch nanocrystal and protein matrix are hydrophilic, it is evident that in these films the interactions between the components, possibly through the formation of hydrogen bridges, would leave fewer sites available to absorb water. The decrease in WU with the addition of nanocrystals could also be due to an increase in film surface hydrophobicity, as was evidenced by increasing contact angle for all measured concentrations of waxy maize starch nanocrystals, and for 6 wt% normal starch nanocrystals. This can be attributed to protein/nanocrystal interactions, leaving a lower concentration of hydrophilic groups exposed towards film surface.

Amaranth protein film showed high water solubility. This behavior could be attributed to occur a reduction of the effectiveness of crosslinking between the peptide chains because the proteins in the film retained partially their native structure (Condés et al., 2013). No significant differences in water solubility were observed with the addition of starch nanocrystals to film formulations, except for the film that contained 12 wt% normal maize starch nanocrystals that presented an increase in its solubility. These results suggest that the interactions between starch nanocrystals and proteins, mainly hydrogen bonds as was reported in the literature (Kristo & Biliaderis, 2007), were able to break under the conditions of films solubility test, so that the presence of nanocrystals was not manifest. But at higher nanocrystal concentrations they could modify the protein crosslinking process, affecting the film solubility.

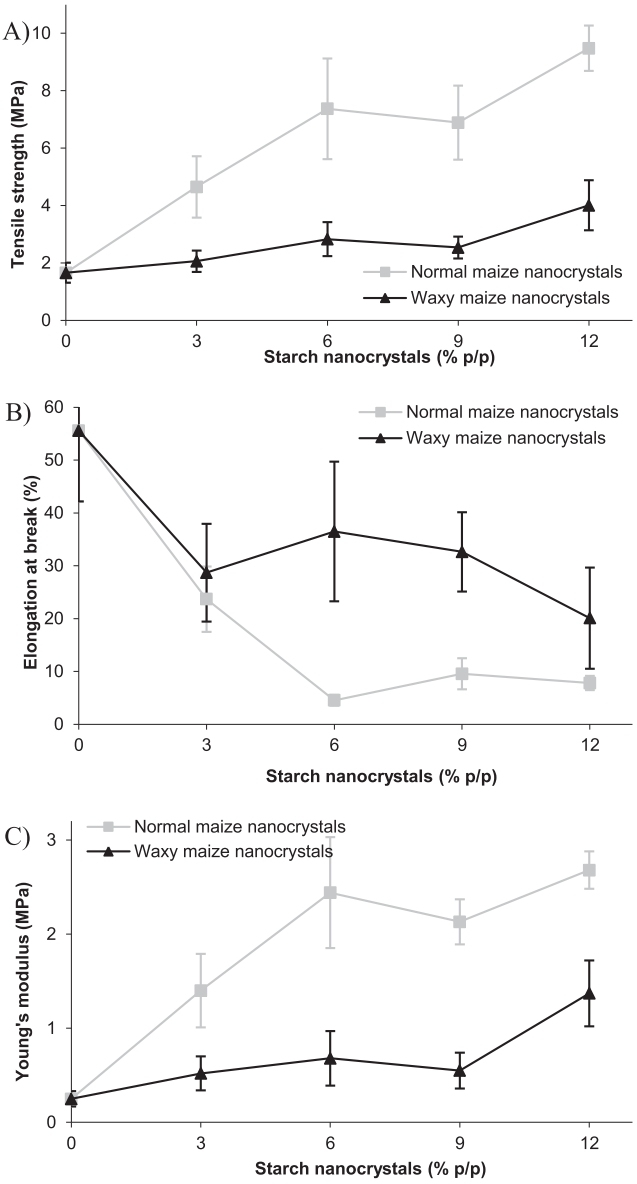

Fig. 4. Mechanical properties: A) tensile strength, B) elongation at break and C) Young's modulus of amaranth protein isolate films with the addition of different contents of normal and waxy maize starch nanocrystals.

3.2.3. Mechanical properties

Fig. 4 shows the evolution of the mechanical properties for protein films upon addition of increasing amounts of nanocrystals prepared from maize starch – normal and waxy.

The neat amaranth protein film exhibited poor mechanical properties: tensile strength about 1.7 MPa, elongation at break of about a 55.6%, and Young's modulus of about 0.3 MPa; values that are found within the same range for other protein films in the literature (Denavi et al., 2009; Echeverría et al., 2014; Tapia-Blácido, Mauri, Menegalli, Sobral, & Añón, 2007).

The tensile strength and Young's modulus for nanocomposites dramatically increased while the elongation at break decreased with starch nanocrystal addition. This effect was more notorious for normal maize starch nanocrystals than for waxy.

When adding normal waxy nanocrystals, the maximum increase of tensile strength and Young's modulus was 470 and 972%, respectively, while when adding waxy maize nanocrystals, the maximum increase was 140 and 450%, respectively. This increase was achieved for 12 wt% of both nanocrystals. Further, with addition of both starch nanocrystals, the elongation at break decreased although more dramatically for normal maize nanocrystals. The reinforcing effect of the nanocrystals to the amaranth protein film could be attributed to the good dispersion and affinity between starch nanocrystals and proteins that result in strong interactions. This affinity was also suggested in the previous section, when analyzing the films thickness, color, opacity, and water uptake. Several authors have attributed the reinforcing effect observed for polymeric films reinforced with starch nanocrystals to their uniform distribution due to their small size and strong interactions that can be formed between nanocrystals and different hydrophilic matrices, such as soy protein isolate, polyvinyl alcohol or various starches (Chen et al., 2008; Viguié, Molina-Boisseau, & Dufresne, 2007; Zheng et al., 2009). However, the effect induced by the nanocrystals on the mechanical properties as well as on other properties, such as susceptibility to water, has a strong dependence on the concentration (LeCorre et al., 2010) and botanical origin of the nanocrystals, and it is variable depending on the matrix used. For example, natural rubber matrix shows improved mechanical properties when adding 20 wt% waxy maize starch nanocrystals (Angellier et al., 2005). In polyurethane films, the maximum

reinforcing effect was observed with 5 wt% potato starch nanocrystals (Chen et al., 2008), and the maximum reinforcement for soy protein matrix was observed with the addition of 2 wt% pea starch nanocrystals (Zheng et al., 2009). In this last case, the authors attributed this behavior to self-aggregation of the nanocrystals as large domains, which decreased the effective surface for interacting with the protein matrix.

The higher reinforcing effect provided by normal maize starch nanocrystals compared to waxy appears quite surprising since the former have lower crystallinity as shown in Table 2. Moreover, stronger interactions seem to exist between the protein matrix and waxy maize starch nanocrystals as attested from solubility and contact angle values (Table 5). The difference in the reinforcing effect of both nanocrystals could be attributed to the higher melting temperature, resulting from a more perfect crystalline arrangement, and smaller aggregate size for normal maize starch nanocrystals (Table 2), and probably to differences in the interactions among proteins and nanocrystals.

3.2.4. Structural properties

In order to further analyze the film structure–function relationship, protein interactions involved in the stabilization of the films prepared from protein isolates and starch nanocrystals were studied. In particular, the differential solubility of film proteins in buffer systems with the capacity to disrupt different types of interactions was studied. Such systems were: water (W), which can dissolve free polypeptides not strongly linked to the protein matrix; phosphate buffer (PB), which affects protein electrostatic interactions; PBD, which contains SDS and disrupt mainly hydrophobic interactions and also interacts with proteins increasing their charge/mass ratio; PBU, which contains urea and disrupts the water structure affecting hydrogen bonds and also hydrophobic interactions; PBDU, which disrupts all the interactions mentioned above and also modifies protein charge; and PBDUM, which also disrupts disulfide bonds because it contains 2-mercaptoethanol. The results obtained for the unfilled protein film and nanocomposites with 6 and 12 wt% nanocrystals are shown in Fig. 5.

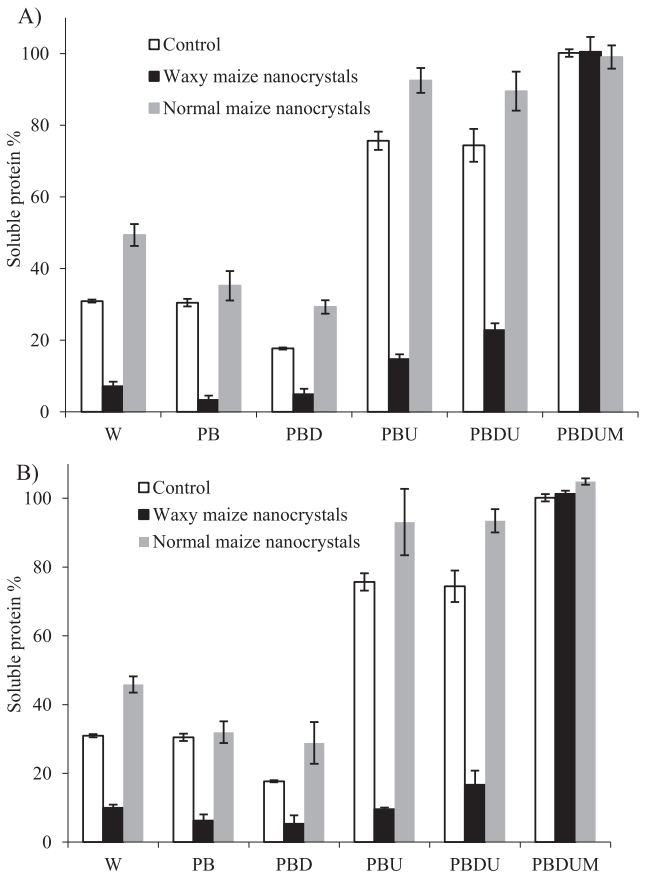

Fig. 5. Differential protein solubility of films prepared from amaranth protein isolates and 6 wt% (A) and 12 wt% (B) normal and waxy maize starch nanocrystals in solvents with different chemical activity: Water (W), 0.1 M sodium phosphate buffer (PB), PB containing 0.1% w/v SDS (PBD), PB containing 6 M urea (PBU), PB containing both 0.1% SDS and 6 M urea (PBDU), and PBDU containing 2.5% v/v, 2-mercaptoethanol (PBDUM), all solutions were at pH 7.5. Values for each protein isolate are expressed as average ± standard deviation.

Protein films are stabilized mainly by electrostatic, hydrogen and disulfide bonds, as evidenced by their higher solubility in buffers PB, PBU and PBDUM. The nanocomposite films showed different solubility profiles than the neat amaranth protein film, but no differences were observed between the corresponding films with the addition of 6 or 12 wt% nanocrystals (Fig. 5A and B).

Proteins in films reinforced with waxy maize starch nanocrystals that showed smooth homogeneous microstructure, presented lower water solubility than proteins in the control film, indicating large amount of interactions that water cannot disrupt between proteins themselves and with nanocrystals. Such solubility was unchanged in PB, but increased slightly when using PBU and PBDU, indicating that the disruption of hydrogen bonds affects the solubility of proteins. However, when the films were exposed to PBDUM all proteins were solubilized. It seems that disulfide bonds among proteins determine protein solubility. The nanocrystals seem to have a good affinity with the protein matrix, since the elongation at break of the films decreased even for low filler contents. This could be because the sites previously interacting among proteins by hydrophobic interactions and hydrogen bonds now interact with the reinforcement, and the buffers used are not capable of breaking these interactions. These interactions can also cause conformational changes in proteins during film formation that favor protein crosslinking through disulfide bonds.

In contrast, protein films reinforced with normal maize starch nanocrystals showed a solubility profile completely different, since film solubilization in all buffers was higher or equal than for the control film, achieving almost 100% solubility in PBU. The presence of these nanocrystals seems to decrease the protein crosslinking, since there is a higher proportion of free polypeptides weakly interacting with the matrix (because of its higher solubility in water), and the disulfide bonds would not favor the integrity of the film. This shows that non-covalent, particularly hydrogen bonds type and electrostatic interactions seem to be the most important in stabilizing the nanocomposite matrix. These films showed better mechanical properties, which could indicate that the strong interaction between the protein matrix and the nanocrystals might be more susceptible to break on the assay conditions or might be responsible for the decrease in protein crosslinking itself.

It has been reported that materials with higher capacity to establish covalent interactions through disulfide bonds form more resistant and stretchable matrices (Pérez-Gago & Krochta, 2001). In the present study, films reinforced with waxy maize starch nanocrystals, in which the disulfide bonds have a more important role in stabilizing the protein matrix, showed higher elongation at break but lower stress resistance. This behavior might be due to the distribution of disulfide bonds in the protein matrix governed by the conformational changes in proteins structure due to the presence of nanocrystals. The glass transition temperature (T_g) of films prepared from amaranth protein isolate, and normal and waxy starch nanocrystals determined by differential scanning calorimetry are shown in Table 6. The T_g value increased about 12 °C when adding 6 wt% normal maize starch nanocrystals or 12 wt% waxy

Table 6
Glass transition temperature (T_g) for films prepared from amaranth protein isolate, and normal and waxy maize starch nanocrystals.

	Starch nanocrystal content (wt%)	T_g (°C)
Control	0	-69 ± 1^a
Normal maize	6	-57 ± 2^b
	12	-57 ± 1^b
Waxy maize	6	-69 ± 1^a
	12	-55 ± 1^b

All values were average ± SD of two values. Reported average values of all parameters within a column with same superscripts (*a* and *b*) are not significantly different ($P < 0.05$).

maize starch nanocrystals. The most marked effect for normal maize starch nanocrystals on the T_g could be correlated with greater effect on mechanical properties.

Similarly, several authors reported a significant increase of T_g for plasticized starch matrix with increasing ramie cellulose nanocrystal, starch nanocrystal and cellulose fiber contents (Angellier, Molina-Boisseau, Dole, & Dufresne, 2006; Avérous, Fringant, & Moro, 2001; Lu, Weng, & Cao, 2006). Therefore, the glass transition temperature shifted towards higher temperatures with increasing amount of nanocrystals, which can be attributed to a restriction of the mobility of protein chains due to the establishment of strong interactions through hydrogen bonding not only between starch nanocrystals but also between the filler and the matrix. Such interfacial H-bonding leads to a strong adsorption of polymer chains on the surface of nanoparticles (Smith, Bedrov, & Smith, 2003) and formation of 'trapped entanglements' of the polymer segments, resulting in the obstruction of mobility not only of polymer chains attached to the particle surface, but also those having no direct contact with the filler surface.

3.2.5. *Biodegradation of films in soil*

Considering that both the matrix and the reinforcement of the studied films are completely biodegradable, biodegradation in soil for films prepared from amaranth protein isolates with 6 and 12 wt % normal maize starch nanocrystals was analyzed, and compared with the behavior of protein films. Fig. 6 shows the relative weight loss of the films and their macroscopic appearance as a function of time of the assay.

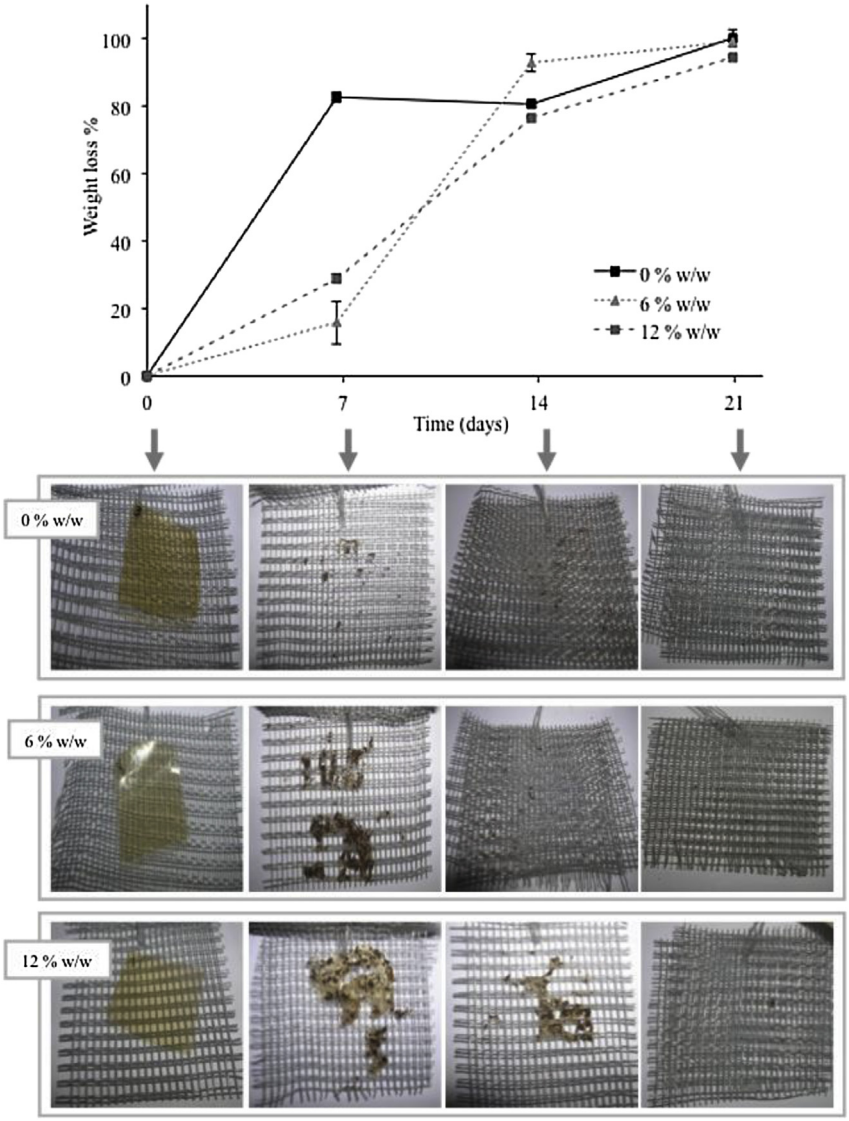

Fig. 6. Weight loss in soil of films prepared from amaranth protein isolate and 0, 6 or 12 wt% of normal maize starch nanocrystals for up to 21 days.

The protein film was the material that biodegraded more quickly, since after one week a weight loss of 80% was observed. In contrast, with addition of 6 wt% and 12 wt% nanocrystals to the matrix, the weight loss was 18% and 28%, respectively. However, after 2 weeks of incubation of the films in soil, the weight loss was almost similar for all films, reaching values between 80 and 90% to total biodegradation after three weeks of exposure. This is clearly observed in the pictures on the macroscopic appearance of the films after incubation. This would indicate that nanocrystals protect the protein matrix from biodegradation at short times. Therefore, the interactions between the nanocrystals and their affinity with the protein matrix, reflected in the properties discussed above, make it more difficult to biodegrade at short times. It should be noted that this system is completely biodisintegrable, because unlike other reinforced nanocomposites, they could also disintegrate. These differences make these films interesting for specific applications.

4. Conclusions

The addition of maize starch nanocrystals to amaranth protein formulations allowed improving the general behavior of protein films, since nanocomposite films presented improved WVP, WU, surface hydrophobicity and mechanical behavior than neat proteins films, without affecting their optical properties and thickness. These materials were also totally biodegradable even though nanocrystals seemed to protect the protein matrix from weight loss in soil at short times. These improvements could be attributed to the good dispersion of the starch nanocrystals in the protein matrix and the good chemical affinity between both components.

Moreover, the botanical origin of starch nanocrystals influenced the reinforcement effect. It was shown that the presence of the nanoreinforcement affected the way in which protein matrix stabilized, mainly by disulfide bonds with waxy maize nanocrystals and by hydrogen bonds with normal maize nanocrystals. This induced a higher reinforcing effect on amaranth protein films, especially for normal maize nanocrystals, that present nevertheless a lower crystallinity.

Acknowledgments

The authors wish to thank the National Agency of Scientific and Technological Support of Argentina (ANPCyT, PICT 2010-1837), and to the CNRS (France) – CONICET (Argentina) Cooperation Project for their financial support.

References

Ai, F., Zheng, H., Wei, M., & Huang, J. (2007). Soy protein plastics reinforced and toughened by SiO_2 nanoparticles. *Journal of Applied Polymer Science, 105*, 1597–1604.

Angellier, H., Choisnard, L., Molina-Boisseau, S., Ozil, P., & Dufresne, A. (2004). Optimization of the preparation of aqueous suspensions of waxy maize starch nanocrystals using a response surface methodology. *Biomacromolecules, 5*, 1545–1551.

Angellier, H., Molina-Boisseau, S., Dole, P., & Dufresne, A. (2006). Thermoplastic starch–waxy maize starch nanocrystals nanocomposites. *Macromolecules, 7*, 531–539.

Angellier, H., Molina-Boisseau, S., & Dufresne, A. (2005). Mechanical properties of waxy maize starch nanocrystal reinforced natural rubber. *Macromolecules, 38*, 9161–9170.

Angellier, H., Putaux, J. L., Molina-Boisseau, S., Dupeyre, D., & Dufresne, A. (2005). Starch nanocrystals fillers in an acrylic polymer matrix. *Macromolecular Symposia, 221*, 95–104.

AOAC 920.53. (1995). *Official methods of analysis* (16th ed.). Gaithersburg, MD: AOAC International.

ASTM D644-94. (1994). Standard test methods for moisture content of paper and paperboard by oven drying. In *Annual book of ASTM standards*. Philadelphia, PA: USA.

ASTM E96-00. (1996). Standard test methods for water vapor transmission of materials. In *Annual book of ASTM*. Philadelphia, PA: USA.

Avérous, L., Fringant, C., & Moro, L. (2001). Plasticized starch–cellulose interactions in polysaccharide composites. *Polymer, 42*, 6565–6572.

Barichello, V., Yada, R. Y., Coffin, R. H., & Stanley, D. W. (1990). Low temperature sweetening in susceptible and resistant potatoes: starch structure and composition. *Journal of Food Science, 54*, 1054–1059.

Bradford, M. M. (1976). A rapid and sensitive method for the quantification of microgram quantities of protein utilizing the principle of protein-dye binding. *Analytical Biochemistry, 72*, 248–254.

Bressani, R. (1989). The proteins of grain amaranth. *Food Reviews International, 5*, 13–38.

Cao, N., Fu, Y., & He, J. (2007). Preparation and physical properties of soy protein isolate and gelatin composite films. *Food Hydrocolloids, 21*, 1153–1162.

Chen, Y., Cao, X., Chang, P. R., & Huneault, M. A. (2008). Comparative study on the films of poly(vinyl alcohol)/pea starch nanocrystals and poly(vinyl alcohol)/native pea starch. *Carbohydrate Polymers, 73*, 8–17.

Chen, P., & Zhang, L. (2006). Interaction and properties of highly exfoliated soy protein/montmorillonite nanocomposites. *Biomacromolecules, 7*, 1700–1706.

Condés, M. C., Añón, M. C., & Mauri, A. N. (2013). Amaranth protein films from thermally treated proteins. *Journal of Food Engineering, 119*, 573–579.

Cuq, B., Gontard, N., & Guilbert, S. (1998). Proteins as agricultural polymers for packaging production. *Cereal Chemistry, 75*, 1–9.

Dalev, P. G., Patil, R. D., Mark, J. E., Vassileva, E., & Fakirov, S. (2000). Biodegradation of chemically modified gelatin films in soil. *Journal of Applied Polymer Science, 78*, 1341–1347.

Dean, K., & Yu, L. (2005). Biodegradable protein-nanoparticle composites. In R. Smith (Ed.), *Biodegradable polymers for industrial applications* (p. 289). Boca Raton, FL: CRC.

Denavi, G., Tapia Blácido, D. R., Añón, M. C., Sobral, P. J. A., Mauri, A. N., & Menegalli, F. C. (2009). Effects of drying conditions on some physical properties of soy protein films. *Journal of Food Engineering, 90*, 341–349.

Duan, B., Sun, P., Wang, X., & Yang, C. (2011). Preparation and properties of starch nanocrystals/carboxymethyl chitosan nanocomposite films. *Starch/Stärke, 63*, 528–535.

Echeverría, I., Eisenberg, P., & Mauri, A. N. (2014). Nanocomposites films based on soy proteins and montmorillonite processed by casting. *Journal of Membrane Science, 449*, 15–26.

Eichhorn, S. J., Dufresne, A., Aranguren, M., Marcovich, N. E., Capadona, J. R., Rowan, S. J., et al. (2010). Review: current international research into cellulose nanofibres and nanocomposites. *Journal of Materials Science, 45*, 1–33.

French, D. (1984). Organization of starch granules. In R. L. Whistler, J. N. BeMiller, & E. F. Paschall (Eds.), *Starch: Chemistry and technology* (pp. 183–247). New York: Academic Press.

García, N., Ribba, L., Dufresne, A., Aranguren, M. I., & Goyanes, S. (2009). Physico-mechanical properties of biodegradable starch nanocomposites. *Macromolecular Materials and Engineering, 294*, 169–177.

Gennadios, A. (2002). *Protein based films and coatings*. Boca Raton, FL: CRC Press.

Gennadios, A., McHugh, T. H., Weller, C. L., & Krochta, J. M. (1994). Edible coatings and film based on proteins. In J. M. Krochta, E. A. Baldwin, & M. Nisperos-Carriedo (Eds.), *Edible coatings and films to improve food quality* (pp. 201–278). Lancaster: Technomic Publishing Co. Inc.

Gontard, N., Guilbert, S., & Cuq, J. (1992). Edible wheat gluten films: influence of the main process variables on films properties using response surface methodology. *Journal of Food Science, 57*, 190–195.

Hanashiro, I., Abe, J., & Hizukuri, S. (1996). A periodic distribution of the chain length of amylopectin as revealed by high-performance anion-exchange chromatography. *Carbohydrate Research, 283*, 151–159.

Jane, J., Chen, Y. Y., Lee, L. F., McPherson, A. E., Wong, K. S., & Radosavljevic, M. (1999). Effects of amylopectin branch chain length and amylose content on the gelatinization and pasting properties of starch. *Cereal Chemistry, 76*, 629–637.

Konishi, Y., & Yoshimoto, N. (1989). Amaranth globulin as a heat-stable emulsifying agent. *Agricultural and Biological Chemistry, 53*, 3327–3328.

Kristo, E., & Biliaderis, C. G. (2007). Physical properties of starch nanocrystal-reinforced pullulan films. *Carbohydrate Polymers, 68*, 146–158.

Krochta, J. M. (1997). Edible protein films and coatings. In S. Damodaran, & A. Paraf (Eds.), *Food proteins and their applications* (pp. 529–549). New York: Marcel Dekker.

LeCorre, D., Bras, J., & Dufresne, A. (2010). Starch nanoparticles: a review. *Biomacromolecules, 11*, 1139–1153.

LeCorre, D., Bras, J., & Dufresne, A. (2011). Influence of botanic origin and amylose content on the morphology of starch nanocrystals. *Journal of Nanoparticle Research, 13*, 7193–7208.

LeCorre, D., Bras, J., & Dufresne, A. (2012). Influence of native starch's properties on starch nanocrystals thermal properties. *Carbohydrate Polymers, 87*, 658–666.

Lehmann, J. W. (1996). Case history of grain amaranth as an alternative crop. *Cereal Foods World, 41*, 399–411.

Lin, N., Huang, J., & Dufresne, A. (2012). Preparation, properties and applications of polysaccharide nanocrystals in advanced functional nanomaterials: a review. *Nanoscale, 4*, 3274–3294.

Ljungberg, N., Bonini, C., Bortolussi, F., Boisson, C., Heux, L., & Cavaille, J. Y. (2005). New nanocomposite materials reinforced with cellulose whiskers in atactic polypropylene: effect of surface and dispersion characteristics. *Biomacromolecules, 6*, 2732–2739.

Lu, Y., Weng, L., & Cao, X. (2006). Morphological, thermal and mechanical properties of ramie crystallites-reinforced plasticized starch biocomposites. *Carbohydrate Polymers, 63*, 198–204.

Martínez, E. N., & Añón, M. C. (1996). Composition and structural characterization of amaranth protein isolates. *Journal Agricultural and Food Chemistry, 44*, 2523–2530.
Mauri, M. N., & Añón, M. C. (2006). Effect of solution pH on solubility and some structural properties of soybean protein isolate films. *Journal of the Science Food and Agriculture, 86*, 1064–1072.
Morrison, W. R., Milligan, T. P., & Azudin, M. N. (1984). A relationship between de amylose and lipids contents of starches from diploid cereals. *Journal of Cereal Science, 2*, 257–260.
Nair, K. G., & Dufresne, A. (2003). Crab shell chitin whisker reinforced natural rubber nanocomposites. 2. Mechanical behaviour. *Biomacromolecules, 4*, 666–674.
Nara, S., & Komiya, T. (1983). Studies on the relationship between water-satured state and crystallinity by the diffraction method for moistened potato starch. *Starch/Starke, 35*, 407–410.
Oates, C. G. (1997). Towards an understanding of starch granule structure and hydrolysis. *Trends in Food Science & Technology, 8*, 375–382.
Paillet, M., & Dufresne, A. (2001). Chitin whiskers reinforced thermoplastic nanocomposites. *Macromolecules, 34*, 6527–6530.
Pérez-Gago, M. B., & Krochta, J. M. (2001). Denaturation time and temperature effects on solubility, tensile properties, and oxygen permeability of whey protein edible films. *Journal of Food Science, 66*, 705–710.
Petersson, L., & Oksman, K. (2006). Biopolymer based nanocomposites: comparing layered silicates and microcrystalline cellulose as nanoreinforcement. *Composites Sciences and Technology, 66*, 2187–2196.
Putaux, J. L., Molina-Boisseau, S., Momaur, T., & Dufresne, A. (2003). Platelet nanocrystals resulting from the disruption of waxy maize starch granules by acid hydrolysis. *Biomacromolecules, 4*, 1198–1202.
Samir Azizi, M. A. S., Alloin, F., & Dufresne, A. (2005). Review of recent research into cellulosic whiskers, their properties and their application in nanocomposite field. *Biomacromolecules, 6*, 612–626.
Sandhu, K. S., Singh, N., & Kaur, M. (2004). Characteristics of the different corn types and their grain fractions: physicochemical, thermal, morphological, and rheological properties of starches. *Journal of Food Engineering, 64*, 119–127.
Singh, N., Inouchi, N., & Nishinari, K. (2006). Structural, thermal and viscoelastic characteristics of starches separated from normal, sugary and waxy maize. *Food Hydrocolloids, 20*, 923–935.
Singh, N., Singh, J., Kaur, L., Sodhi, N. S., & Gill, B. S. (2003). Morphological, thermal and rheological properties of starches from different botanical sources. *Food Chemistry, 81*, 219–231.
Smith, J. S., Bedrov, D., & Smith, G. D. (2003). A molecular dynamics simulation study of nanoparticle interactions in a model polymer–nanoparticle composite. *Composites Sciences and Technology, 63*, 1599–1605.
Sobral, P. J. A., Menegalli, F. C., Hubinger, M. D., & Roques, M. A. (2001). Mechanical water vapor barrier and thermal properties of gelatin based edible films. *Food Hydrocolloids, 15*, 423–432.
Tang, H., Mitsunaga, T., & Kawamura, Y. (2006). Molecular arrangement in blocklets and starch granule architecture. *Carbohydrate Polymers, 63*, 555–560.
Tapia-Blácido, D., Mauri, A. N., Menegalli, F. C., Sobral, P. J. A., & Añón, M. C. (2007). Contribution of the starch, protein, and lipid fractions to the physical, thermal, and structural properties of amaranth (*Amaranthus caudatus*) flour films. *Journal of Food Science, 72*, 293–300.
Tester, R. F. (1997). Starch: the polysaccharide fractions. In P. J. Frazier, P. Richmond, & A. M. Donald (Eds.), *Starch, structure and functionality* (pp. 163–171). Royal Society of Chemistry.
Thielemans, W., Belgacem, M. N., & Dufresne, A. (2006). Starch nanocrystals with large chain surface modifications. *Langmuir, 22*, 4804–4810.
Viguié, J., Molina-Boisseau, S., & Dufresne, A. (2007). Processing and characterization of waxy maize starch films plasticized by sorbitol and reinforced with starch nanocrystals. *Macromolecular Bioscience, 7*, 1206–1216.
Williams, P. C., Kuzina, F. D., & Hlynka, I. (1970). A rapid calorimetric procedure for estimating the amylose content of starches and flours. *Cereal Chemistry, 47*, 411–420.
Yoo, S., & Jane, J. (2002). Structural and physical characteristics of waxy and other wheat starches. *Carbohydrate Polymers, 49*, 297–305.
Yu, J., Cui, G., Wei, M., & Huang, J. (2007). Facile exfoliation of rectorite nanoplatelets in soy protein matrix and reinforced bionanocomposites thereof. *Journal of Applied Polymer Science, 104*, 3367–3377.
Yu, L., Dean, K., & Li, L. (2006). Polymer blends and composites from renewable resources. *Progress in Polymer Science, 31*, 576–602.
Zheng, H., Ai, F., Chang, P. R., Huang, J., & Dufresne, A. (2009). Structure and properties of starch nanocrystal-reinforced soy protein plastics. *Polymer Composites, 30*, 474–480.
Zheng, H., Ai, F., Wei, M., Huang, J., & Chang, P. R. (2007). Thermoplastic soy protein nanocomposites reinforced by carbon nanotubes. *Macromolecular Materials and Engineering, 292*, 780–788.
Zobel, H. F. (1988). Starch crystal transformations and their industrial importance. *Starch, 40*, 1–7.
Zobel, H. F., Young, S. N., & Rocca, L. A. (1988). Starch gelatinization: an X-ray diffraction study. *Cereal Chemistry, 65*, 443–446.